

## A three-dimensional manganese(II) coordination polymer: synthesis, structure and catecholase activity

Prama Bhattacharjee, Partha Mitra, Prasenjit Sarkar & Rohith P. John

To cite this article: Prama Bhattacharjee, Partha Mitra, Prasenjit Sarkar & Rohith P. John (2020): A three-dimensional manganese(II) coordination polymer: synthesis, structure and catecholase activity, Journal of Coordination Chemistry, DOI: [10.1080/00958972.2020.1740213](https://doi.org/10.1080/00958972.2020.1740213)

To link to this article: <https://doi.org/10.1080/00958972.2020.1740213>

 View supplementary material 

 Published online: 23 Mar 2020.

 Submit your article to this journal 

 Article views: 2

 View related articles 

 View Crossmark data 



## A three-dimensional manganese(II) coordination polymer: synthesis, structure and catecholase activity

Prama Bhattacharjee<sup>a</sup>, Partha Mitra<sup>b</sup>, Prasenjit Sarkar<sup>c</sup> and Rohith P. John<sup>a</sup> 

<sup>a</sup>Department of Chemistry, Indian Institute of Technology (ISM), Dhanbad, Jharkhand, India;

<sup>b</sup>Department of Central Scientific Service, Indian Association for Cultivation of Science, Kolkata, India;

<sup>c</sup>Department of Chemistry, Indian Institute of Technology Guwahati, Guwahati, Assam, India

### ABSTRACT

A manganese-based coordination polymer,  $[\text{Mn}_2\text{L}_2(\mu\text{-MeOH})_2]_n$  ( $\text{H}_2\text{L} = 2\text{-hydroxy-1-naphthaldehyde isonicotinoylhydrazone}$ ) was obtained by self-assembly of 2-hydroxy-1-naphthaldehyde isonicotinoylhydrazone and manganese(II) acetate. The coordination polymer was characterized by IR, EPR and UV-Vis spectroscopy. The single-crystal X-ray diffraction study reveals that the dibasic tridentate ligand ( $\text{L}^{2-}$ ) is bound *via* ONO donor sites to manganese(II). Two such [ML] fragments are connected by  $\mu_2$ -bridged methanol (MeOH) to form a di-manganese species. The sixth site of each of the manganese is occupied by the pyridyl N atom of the isonicotinoyl group. This arrangement gives a polynuclear complex of the formula  $[\text{Mn}_2\text{L}_2(\mu\text{-MeOH})_2]_n$ . The coordination geometry of manganese is distorted octahedral. The X-band electron paramagnetic resonance (EPR) measurement of the complex at 77 K shows a six-line spectrum and a signal at the half field, with  $g = 4.88$ . The half-field signal indicates the dimeric nature of the complex in the solution state. The cyclic voltammetric measurement of the complex shows a reversible  $\text{Mn}^{\text{III}}/\text{Mn}^{\text{II}}$  redox couple. The complex catalyzes the conversion of 3,5-di-*tert*-butyl catechol to the corresponding *o*-quinone with a catalytic turnover rate of ( $k_{\text{cat}}$ )  $27.22 \text{ h}^{-1}$ .

### ARTICLE HISTORY

Received 2 October 2019

Accepted 18 February 2020

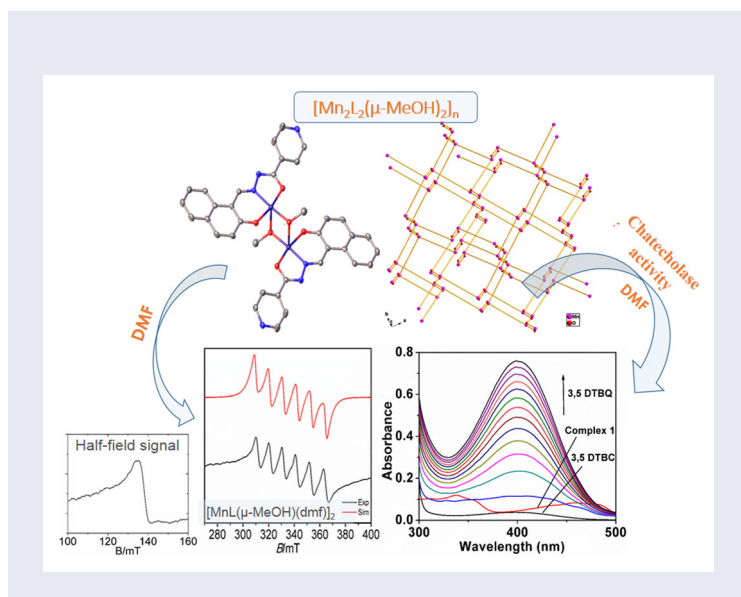
### KEYWORDS

Coordination polymer; EPR spectra; manganese; catecholase activity; cyclic voltammetry

**CONTACT** Rohith P. John  [rohithjohn@iitism.ac.in](mailto:rohithjohn@iitism.ac.in)  Department of Chemistry, Indian Institute of Technology (ISM), Dhanbad, Jharkhand, 826004, India

 Supplemental data for this article is available online at <https://doi.org/10.1080/00958972.2020.1740213>.

© 2020 Informa UK Limited, trading as Taylor & Francis Group



## 1. Introduction

Manganese is a metal which can readily shuttle between oxidation states +2 and +3. This behavior is widely utilized in redox metalloenzymes, such as catalase, ribonucleotide reductase, superoxide dismutase and dioxygenase [1]. Manganese enzymes have various types of active sites having different nuclearity, including the tetranuclear manganese clusters that exist at the reactive site of photosynthetic water oxidation [2]. This has led researchers to develop manganese complexes of different nuclearity not only to develop better and efficient catalysts, but also in the design of single-molecule magnets [3]. Several multinuclear manganese complexes with diverse structures such as rings [4], clusters and coordination polymers have been studied, owing to their structural diversity [5], magnetism [6], sensing [7] and catalysis [8]. The choice of manganese in many such synthetic models is due to the fact that it is a redox-active metal ion, has flexible coordination geometry and therefore offers plenty of choice for structural modulation [9–11]. Dinuclear manganese complexes are widely utilized for various catalytic conversions, such as epoxidation, hydroxylation, and hydrosilylation/hydrogermylation [12–15]. Polynuclear manganese complexes also show interesting magnetic anisotropy properties [16]. In addition, various multinuclear manganese complexes are also shown to catalyze conversions such as oxygen transfer reactions and water oxidation [17, 18].

In recent years many of the manganese complexes were shown to catalyze superoxide-dismutase-like activity and catecholase activity [19, 20]. The two major metalloenzymes, catechol dioxygenase and catechol oxidase, catalyze the conversion of catechol to their respective products [21, 22]. Catechol oxidase is generally found in some plants, algae and fungi and catalyzes the oxidation of *o*-diphenols to the corresponding *o*-quinones in the presence of molecular oxygen which gets reduced to

water. The conversion of catechols into *o*-quinones is important as the latter is used in many antiseptic formulations. Although catechol oxidase has a dicopper active site structure, several transition metal complexes with manganese [23], iron [24] and cobalt [25] have been reported to show catecholase activity. Among manganese complexes that display catecholase activity, several have a dinuclear core with alkoxy/phenolate/oxido/methanol bridges [26]. Various strategies are used to generate a dinuclear Mn-Mn core in a polymeric matrix. However, simple strategies such as housing a dinuclear core in a matrix of a coordination polymer that offers voids for the diffusion of the substrate can be very effective. Herein we report a manganese coordination polymer that offers dinuclear Mn ... Mn core bridged methanol molecules obtained by the process of self-assembly.

## 2. Experimental

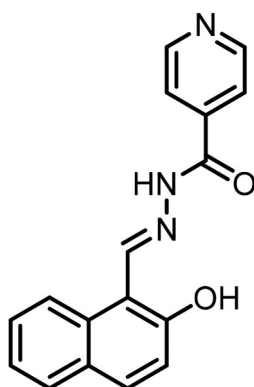
### 2.1. General remarks

All reactions were performed under aerobic conditions. Solvents used for the synthesis were purchased from RANKEM of analytical grade and used after purifying by standard methods. Isonicotinichydrazide and 2-hydroxy-1-naphthaldehyde were purchased from TCI Chemicals and manganese(II) acetate tetrahydrate was purchased from Merck India and were used without purification.

A Perkin Elmer Spectrum-II FT-IR spectrometer was used for infrared spectral measurements. UV-visible spectrum were recorded in *N,N*-dimethyl formamide (DMF) on a Shimadzu UV-2450 spectrometer. Elemental analyses were performed on a Vario Micro cube for C, H, N, S Analyser by Elemental Analyser System GMBH. ESI-Mass spectra were recorded on a VARIAN 410 Prostar Binary LC with 500MS IT PDA in positive mode at SAIF, Punjab University, Chandigarh. The XPS measurement was carried out on a VG Scientific ESCALAB 250 instrument. The cyclic voltammogram was recorded in a CHI1140C electrochemical analyzer equipped with a platinum wire counter electrode, a calomel reference electrode and a glassy carbon disk working electrode. The working electrode was polished before each voltammogram with a 1  $\mu\text{m}$  diamond paste, sonicated in ethyl alcohol, washed with the same solvent, and dried in air. The electrochemical studies were carried out with sample concentrations of 0.5 mM, 0.75 mM and 1 mM in dry DMF (ACROS) using 0.1 M tetrabutylammonium perchlorate (TBAP) as a supporting electrolyte. Nitrogen was purged into the solution for 15 minutes before the start of the experiment. The temperature was maintained with a Julabo circulation bath at 25 °C. The EPR spectrum was recorded at 77 K in DMF on a JEOL ESR Spectrometer at 9.5mW microwave frequency with a fieldset of 330 mT and 200 mT field sweep. EASYSPIIN 5.0.16 was used for EPR simulations [27].

### 2.2. Synthesis of ligand ( $H_2L$ )

The ligand (E)-*N'*-((2-hydroxynaphthalen-1-yl)methylene)isonicotinohydrazide ( $H_2L$ , Scheme 1) was synthesized by condensation of isonicotinichydrazide and 2-hydroxy-1-naphthaldehyde as reported elsewhere [28]. Isonicotinichydrazide (500 mg, 3.64 mmol) and 2-hydroxynaphthaldehyde (627 mg, 3.64 mmol) were taken in 35 mL ethanol



**Scheme 1.** Schematic diagram of H<sub>2</sub>L.

solution and refluxed for 4 h. Upon completion of the reaction, a yellow precipitate was obtained, which was filtered off, washed with ethanol solution and dried under vacuum. 375 mg (75%). <sup>1</sup>H-NMR (DMSO *d*<sub>6</sub>), 25 °C, 400 MHz): (ppm) 12.51 (s, 1H, OH<sub>d</sub>), 12.40 (s, 1H, NH<sub>b</sub>), 9.47 (s, 1H, N=C-H<sub>c</sub>), 8.83 (d, 2H, CH<sub>d</sub>), 8.31 (d, 1H, CH<sub>e</sub>), 7.91 (d, 1H, CH<sub>f</sub>), 7.94 (d, 1H, CH<sub>g</sub>), 7.88 (d, 2H, CH<sub>h</sub>), 7.61 (t, 1H, CH<sub>i</sub>), 7.41 (t, 1H, CH<sub>j</sub>), 7.24 (d, 1H, CH<sub>k</sub>), FT-IR (KBr, cm<sup>-1</sup>): H<sub>2</sub>L, 3226s (-NH), 3029m (aromatic -CH), 1680s (>C=O), 1660m (>C=N), 1286 (>C-O), 1186m (-C-N). Elemental analysis, Anal. Calcd (C<sub>17</sub>H<sub>13</sub>N<sub>3</sub>O<sub>2</sub>): C 70.09, H 4.50, N 14.42, found: C 70.05, H 4.60, N 14.44. ESI-MS: (m/z) 292.30 [M + H]<sup>+</sup>.

### 2.3. Synthesis of {poly[bis(μ-((E)-N'-((2-hydroxynaphthalen-1-yl)methylene)isonicotinohydrazido-κ<sup>4</sup>O<sup>1</sup>:N<sup>1</sup>:O<sup>2</sup>:N<sup>3</sup>)bis(μ-methanol-κ<sup>2</sup>O:O)dimanganese(II)]} (1)

A methanolic solution (4 mL) of Mn(OAc)<sub>2</sub>·4H<sub>2</sub>O (12 mg, 0.05 mmol) and a DMF solution (2 mL) of H<sub>2</sub>L (15 mg, 0.05 mmol) were prepared [29, 30]. The methanolic solution of manganese acetate tetrahydrate was carefully layered over the DMF solution of the ligand. Brown crystals were obtained after 30 days. 8.5 mg (70%). They were used for further characterization. FT-IR (KBr, cm<sup>-1</sup>): Complex **1** 3029 (aromatic -CH), 1667 (>C=O), 1614 (>C=N<sup>2</sup>), 1596 (>C=N<sup>1</sup>), 1332 (C-N), 1194 (C-O), 535 (Mn-O), 493 (Mn-N). UV-Vis for **1** (DMF, λ<sub>max</sub>, nm): π-π\*(314–327 nm), n-π\*(337–400 nm). Elemental analysis: Anal. calcd {[MnL(μ-MeOH)]<sub>2</sub>}<sub>n</sub>·2n(H<sub>2</sub>O): C 54.83, H 4.35, N 10.66%, found: C 55.05, H 4.50, N 10.52%.

### 2.4. X-ray crystallography

The data of **1** were collected at 150K in a Bruker SMART APEX II CCD detector and graphite-monochromatic Mo Kα radiation (λ = 0.71073) at low temperature. The structure was solved by direct methods using SHELXT [31] and refined on F<sup>2</sup> by full-matrix least-squares methods using SHELXL [32]. Non-hydrogen atoms were refined anisotropically. H-atoms were allowed to ride on their respective atoms with U<sub>ij</sub> values -1.2 for aromatic CH groups. The SQUEEZE routine [33] in PLATON was used to remove the electron density distributed in voids. The hydrogen atom attached to the oxygen of

coordinated methanol molecules could not be identified from difference fourier. The SQUEEZE routine was able to recover 364 electrons per unit cell, equivalent to one methanol and 0.5 water molecule per asymmetric unit as disordered solvent accommodated in the solvent-accessible void. The final R (all data) values converged to  $R1 = 0.0456$  and  $wR2 = 0.0834$ .

### 3. Results and discussion

#### 3.1. Synthesis and general spectroscopic characterization

The ligand ( $H_2L$ ) (E)-N'-((2-hydroxynaphthalen-1-yl)methylene)isonicotinohydrazide was synthesized by condensation of isonicotinichydrazide with 2-hydroxy-1-naphthaldehyde as per the reported literature [28]. The mass spectrum of the ligand is consistent with the expected molecular mass of the compound (Figure S1, Supporting Information). The  $^1H$  NMR spectrum of the ligand shows a sharp peak at 12.51 and 12.40 ppm for OH and NH protons, respectively, and the peaks in the range 9.47 to 7.22 ppm can be assigned to aromatic protons (Figure S2, Supporting Information). The IR spectrum of  $H_2L$  displays a broad band at  $3436\text{ cm}^{-1}$  which is due to the asymmetric stretching of the naphthol -OH group, while the band at  $3226\text{ cm}^{-1}$  is due to the hydrazinic -NH stretching (Figure S3, Supporting Information). In **1**, the broad band at  $3428\text{ cm}^{-1}$  may be due to the presence of hydrogen-bonded water molecules trapped in the lattice. The ligand displays a strong band at  $1680\text{ cm}^{-1}$  corresponding to  $>C=O$  stretching, which disappeared in **1**, owing to the enolisation. The band at  $1660\text{ cm}^{-1}$  corresponding to the  $>C=N-$  stretching frequency in the ligand is shifted to  $1596\text{ cm}^{-1}$  in **1**, indicating coordination of azomethine nitrogen atom. The band at  $1614\text{ cm}^{-1}$  may arise from the newly formed  $>C=N-$  bond. The UV-visible spectrum of the ligand shows bands at 326 nm and 363 nm and a shoulder at 374 nm. These bands can be assigned to the  $n-\pi^*$  transition in the ligand backbone and the azomethine group. A series of three bands observed at 439 nm, 466 nm and 496 nm are characteristic of the  $\pi-\pi^*$  transitions of the naphthyl group [34]. The nature and position of the latter set of bands depend on strong intramolecular hydrogen bonding between the hydroxyl group of the naphthyl group and the azomethine nitrogen [35]. The UV-visible spectrum of the complex (Figure S4, Supporting Information) show bands at 338 nm and 352 nm corresponding to  $n-\pi^*$  transitions, while the bands at 430 nm, 460 nm and 478 nm may result from the coordinated azomethine group and modification of the energy of the naphthyl backbone upon coordination [12]. The XPS spectrum of **1** shows (Figure S5, Supporting Information) peaks at 642.3 and 654.8 eV which correspond to the binding energies of the spin-orbit splitting components of Mn  $2p_{3/2}$  and  $2p_{1/2}$ , respectively, in the +2 oxidation state of the metal. The value of Mn  $2p_{3/2}$  is slightly shifted to higher binding energy due to the bonding of the metal with higher electronegativity atoms [36, 37].

#### 3.2. X-ray diffraction studies

The molecular structure of **1** with the atom numbering scheme is shown in Figure 1. Crystallographic refinement parameters are provided in Table 1. Important bond

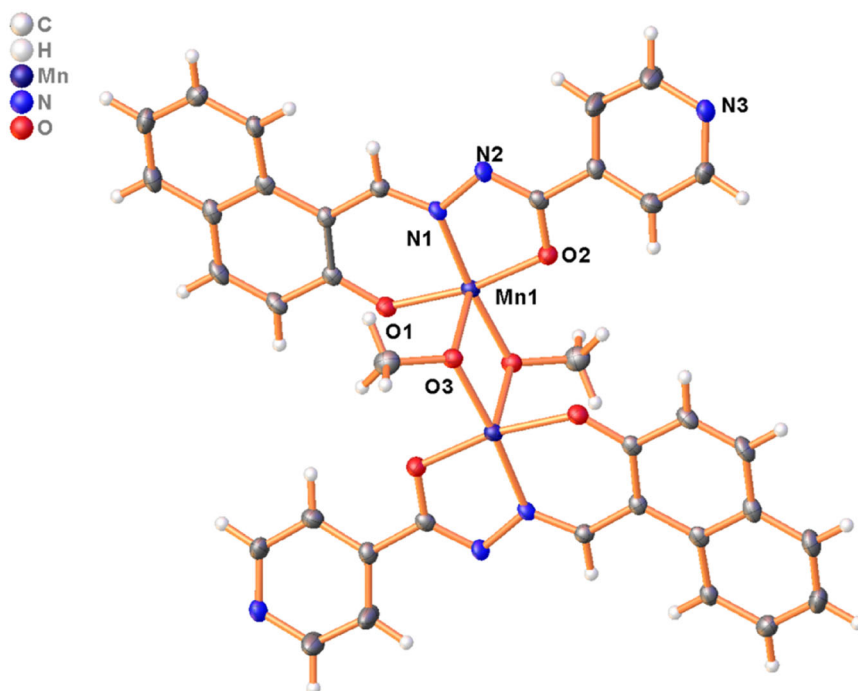


**Figure 1.** A plot of the repeating unit of **1** drawn with 50% probability ellipsoid.

**Table 1.** Crystal data and structure refinement for **1**.

Empirical formula	$C_{36}H_{30}Mn_2N_6O_6$
Formula weight	752.54
Temperature/K	150(2)
Wavelength/Å	0.71073
Crystal system	Tetragonal
Space group	$I 4_1/a$
Unit cell dimensions	$a = 29.1685(13) \text{ \AA}, \alpha = \beta = \gamma = 90^\circ$ $b = 29.1685(13) \text{ \AA}$ $c = 8.8458(5) \text{ \AA}$
Volume/Å <sup>3</sup>	7526.0(8)
Z	8
Density/Mg/m <sup>3</sup>	1.328
Absorption coefficient/mm <sup>-1</sup>	0.721
F(000)	3088
Crystal size/ mm <sup>3</sup>	0.200 × 0.160 × 0.120
Theta range for data collection/ °	1.396 to 25.436
Index ranges	$-35 \leq h \leq 35, -35 \leq k \leq 35, -10 \leq l \leq 10$
Reflections collected	36361
Independent reflections	3484 [R(int) = 0.0684]
Completeness to theta = 25.242°	100.0%
Absorption correction	Semi-empirical from equivalents
Max. and min. transmission	0.916 and 0.868
Refinement method	Full-matrix least-squares on F <sup>2</sup>
Data/restraints/parameters	3484/0/227
Goodness-of-fit on F <sup>2</sup>	1.066
Final R indices [I > 2sigma(I)]	R1 = 0.0325, wR2 = 0.0795
R indices (all data)	R1 = 0.0456, wR2 = 0.0834
Largest diff. peak and hole	0.521 and $-0.343 \text{ e. \AA}^{-3}$

**Table 2.** Selected bond lengths (Å) and angles (°) for **1**.

Bond lengths (Å)			
Mn(1)-O(3)	1.8994(15)	Mn(1)-N(1)	1.9671(18)
Mn(1)-O(1)	1.9159(14)	Mn(1)-O(3) <sup>a</sup>	2.2428(14)
Mn(1)-O(2)	1.9199(14)	Mn(1)-N(3) <sup>b</sup>	2.3662(18)
Bond angles (°)			
O(3)-Mn(1)-O(1)	97.73(6)	O(1)-Mn(1)-N(3) <sup>b</sup>	86.82(6)
O(3)-Mn(1)-O(2)	93.72(6)	O(2)-Mn(1)-N(3) <sup>b</sup>	91.48(6)
O(1)-Mn(1)-O(2)	168.48(6)	N(1)-Mn(1)-N(3) <sup>b</sup>	89.46(7)
O(3)-Mn(1)-N(1)	173.08(7)	O(3) <sup>a</sup> -Mn(1)-N(3) <sup>b</sup>	171.62(6)
O(1)-Mn(1)-N(1)	89.00(7)	O(3)-Mn(1)-Mn(1) <sup>a</sup>	44.82(4)
O(2)-Mn(1)-N(1)	79.59(6)	O(1)-Mn(1)-Mn(1) <sup>a</sup>	93.38(5)
O(3)-Mn(1)-O(3) <sup>a</sup>	81.48(6)	O(2)-Mn(1)-Mn(1) <sup>a</sup>	95.61(5)
O(1)-Mn(1)-O(3) <sup>a</sup>	88.21(6)	N(1)-Mn(1)-Mn(1) <sup>a</sup>	133.53(5)
O(2)-Mn(1)-O(3) <sup>a</sup>	94.72(6)	O(3) <sup>a</sup> -Mn(1)-Mn(1) <sup>a</sup>	36.66(4)
N(1)-Mn(1)-O(3) <sup>a</sup>	97.21(6)	N(3) <sup>b</sup> -Mn(1)-Mn(1) <sup>a</sup>	137.01(5)
O(3)-Mn(1)-N(3) <sup>b</sup>	92.50(6)		

Symmetry transformations used to generate equivalent atoms: <sup>a</sup>-x + 1/2, -y + 1/2, -z + 1/2, <sup>b</sup>-x + 3/4, y - 1/4, z - 1/4.

lengths and angles are listed in Table 2. A thermal ellipsoidal plot of the [Mn<sub>2</sub>L<sub>2</sub>(μ-MeOH)<sub>2</sub>] repeating unit of **1** is shown in Figure 1.

The crystal structure determination of **1**, [Mn<sub>2</sub>L<sub>2</sub>(μ-MeOH)<sub>2</sub>]<sub>n</sub>, reveals that the doubly deprotonated ligand (L<sup>2-</sup>) binds with ONO donor atoms *viz*, phenolate oxygen atom (O1), one imine nitrogen atom (N1) and one oxygen atom (O2). The metal ion is further coordinated by two methanol molecules in a μ<sub>2</sub>-bridging mode. The sixth coordination site of Mn(II) is bound by the pyridine nitrogen atom (N3) of another ligand unit (Figure S6, Supporting Information). The equatorial bond lengths Mn-O1, Mn-O2, Mn-O3 and Mn-N1 are 1.9159(14), 1.9199(14), 1.8994(15) and 1.9671(18) Å, respectively. However, the axial bond lengths Mn-O3<sup>a</sup> (*a* = x + 1/2, -y + 1/2, -z + 1/2) and Mn-N3<sup>b</sup> (*b* = y - 1/4, -x + 3/4, z - 1/4) are 2.2428(14) and 2.3662(18) Å, respectively, indicating axial elongation. The bond lengths are consistent with Mn-O bond lengths of low-spin manganese(II) complexes reported elsewhere (Table S1, see Supporting Information) [38]. The values of distorted octahedral geometry of this Mn complex are satisfied by the bond angles (O3-Mn1-O1 = 97.73(6)°, O1-Mn1-O3<sup>a</sup> (*a* = x + 1/2, -y + 1/2, -z + 1/2) = 88.21(6)°, O3-Mn1-N1 = 173.08(7)°, N1-Mn1-O3<sup>a</sup> (*a* = x + 1/2, -y + 1/2, -z + 1/2) = 97.21(6)°. The distortion can also be gauged from the angle variance (σ<sub>oct</sub>) and quadratic elongation parameter (λ<sub>oct</sub>) whose values, 31.95(°)<sup>2</sup> and 1.024, respectively, indicate moderate distortion. The pyridyl ring is twisted compared to the rest of the metal-ligand moiety with the dihedral angle 14.77° in the asymmetric unit of the coordination polymer. The bridging of the methanol molecules leads to formation of the Mn<sub>2</sub>O<sub>2</sub> dimanganese center with a Mn...Mn distance of 3.146 Å. The Mn-O-Mn angle measures 98.52°, which falls within the range reported for other dinuclear complexes having low-spin Mn(II) at the core [26d-f]. The dimanganese [Mn<sub>2</sub>L<sub>2</sub>(μ-MeOH)<sub>2</sub>] units are connected to other similar units via the pyridyl N3 atom of the isonicotinoyl group. Each Mn<sub>2</sub>O<sub>2</sub> unit acts as a node and leads to a puckered 4-connected closed loop; each such closed loop is further connected to each other via an N3 atom of a pyridyl group of the isonicotinic moiety. These inter-loop connectivity leads to a square-like cavity propagating along the *c*-direction in a helical fashion. Strong π-π stacking interactions and

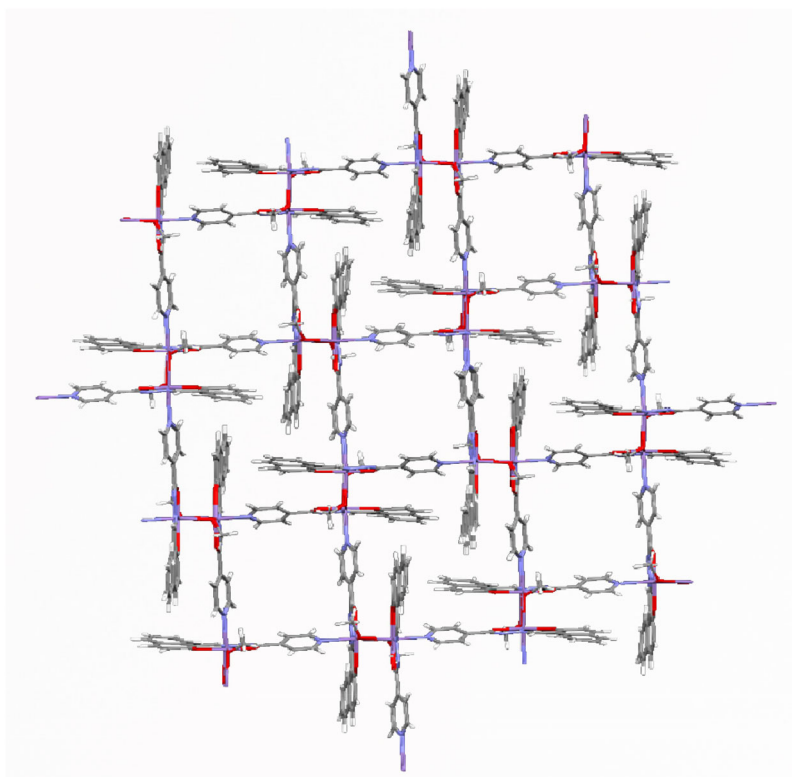


**Figure 2.** A diagram showing the clustering of the naphthyl groups in **1**.

favorable C-H...  $\pi$  interactions appear to stabilize the coordination polymer (Table S2 and Figure S7, see Supporting Information). These interactions favor a clustering of naphthyl groups along the channels formed by 4-connected closed loops, while the helical channels appear to hold solvent molecules along the 4-fold screw axis (Figure 2). The program PLATON finds a solvent-accessible void corresponding to 422 ( $\text{\AA}^3$ ), and an unresolved electron density of 91 electrons, which can be roughly estimated to the presence of four methanol and two water molecules in each of the 4-fold helical channel. Partial network connectivity of this coordination polymer is shown in Figure 3.

### 3.3. Epr study of **1**

The solid-state EPR spectrum of the sample at room temperature gives a broad signal with  $g_{\text{iso}} = 2.023$ , indicating the presence of a weakly coupled manganese(II) dinuclear center (Figure S8, Supporting Information) [39]. To understand the integrity of **1** in solution, the X-band EPR spectrum was measured at 77 K in DMF (Figure 4). The EPR spectrum is anisotropic, giving a well resolved six-line signal. The EPR simulation with  $l = 5/2$  gives a best-fit with the parameters  $g_x = 2.005$ ,  $g_y = 2.010$ ,  $g_z = 2.0015$  and  $g_{\text{iso}} = 2.005$ . This anisotropy is known to arise due to the presence of distortion in the molecular geometry from the perfect octahedral symmetry [40]. The appearance of six lines indicates the coupling of the electronic spin of Mn(II), to the nuclear spin of

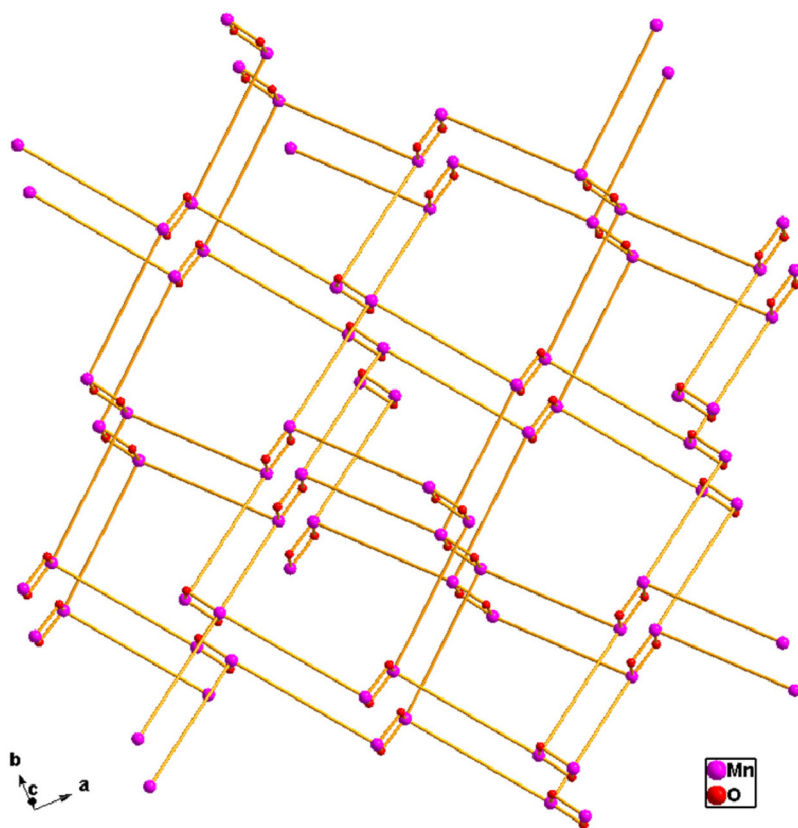


**Figure 3.** A simplified network connectivity of 1.

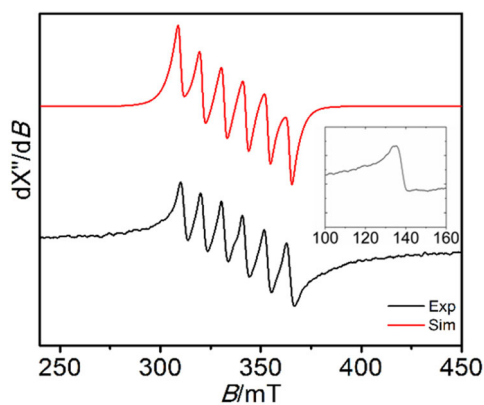


**Figure 4.** The X-band EPR spectrum of 1 recorded at 77 K in DMF. Experimental (black) and simulated (red). Inset: half-field signal of 1.

$^{55}\text{Mn}$  ( $I = 5/2$ ) and that the contribution from axial zero-field splitting parameter ( $D$ ) is marginal. The hyperfine coupling constants  $A_x = 75$ ,  $A_y = 36$ ,  $A_z = 95$  ( $\times 10^{-4} \text{ cm}^{-1}$ ) indicate that the electronic delocalization is not equivalent in the bonds formed by

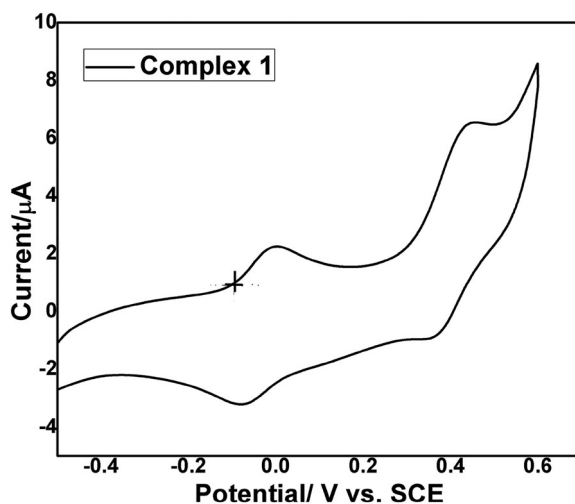


**Figure 5.** Cyclic voltammogram of **1** (0.75 mM) with scan rate  $100 \text{ mVs}^{-1}$  in DMF. (The resting potential is indicated by + mark).

manganese(II) [41]. The weak signal observed at half-field with  $g$  value 4.88 can be inferred as arising from the methanol-bridged dinuclear Mn ... Mn core.

### 3.4. Electrochemical study of **1**

Cyclic voltammetry is widely used to study the redox properties of transition metal complexes. Therefore, the redox properties of **1** were investigated using cyclic voltammetry. The complex dissolves appreciably only in DMF and has limited solubility in acetonitrile and methanol. Hence, the cyclic voltammogram of **1** at a concentration of 0.75 mM was recorded in dry DMF containing 0.1 M  $[(^t\text{Bu})_4\text{N}]\text{ClO}_4$  as supporting electrolyte in a three-electrode system containing glassy carbon electrode as a working electrode, a platinum wire as counter electrode and calomel electrode as a reference electrode. In order to have an idea about the oxidation state of the manganese present, the resting potential of the complex was obtained. The value of  $-0.09 \text{ V}$  indicates that the manganese metal ion is in +2 oxidation state. A cyclic voltammetric potential sweep was performed in the potential range  $+0.5 \text{ V}$  to  $-0.6 \text{ V}$  vs. SCE at  $100 \text{ mV s}^{-1}$  to minimize the interference, owing to ligand-based redox processes which occurs beyond this range (Figure 5). Cyclic voltammetric scan of **1** at different scan rates of 50, 100, 150 and  $200 \text{ mVs}^{-1}$  were performed within the same potential range (Figure S9, Supporting Information) to check the redox property of the manganese complex. The experiment was performed with anodic scan first, followed by cathodic scan. The solution of **1** in DMF displays a quasi-reversible one-electron redox process at  $E_{1/2} = -0.03 \text{ V}$  corresponding to the  $\text{Mn}^{\text{II}}\text{-Mn}^{\text{II}}/\text{Mn}^{\text{II}}\text{-Mn}^{\text{III}}$  redox couple and another one at  $E_{1/2} = +0.4 \text{ V}$  originating from the  $\text{Mn}^{\text{II}}\text{-Mn}^{\text{III}}/\text{Mn}^{\text{III}}\text{-Mn}^{\text{III}}$  redox couple. The anodic scan gives a peak for the  $\text{Mn}^{\text{II}}/\text{Mn}^{\text{III}}$  redox couple at  $E_{\text{pa}} = -0.0046 \text{ V}$  and the cathodic scan gives a peak at  $E_{\text{pc}} = -0.07 \text{ V}$  with a peak to peak separation of ( $\Delta E_{\text{p}} = E_{\text{pa}} - E_{\text{pc}}$ )  $65 \text{ mV}$  for  $\text{Mn}^{\text{III}}/\text{Mn}^{\text{III}}$  redox couple at  $E_{\text{pa}} = +0.43 \text{ V}$  and the cathodic scan gives a peak at  $E_{\text{pc}} = +0.37 \text{ V}$  with a peak to peak separation of ( $\Delta E_{\text{p}} = E_{\text{pa}} - E_{\text{pc}}$ )  $100 \text{ mV}$ . The peak current ratio,  $I_{\text{pa}}/I_{\text{pc}} = 0.71, 0.83$  and  $E_{1/2} = -0.03$  and  $+0.4 \text{ V}$  vs. SCE, respectively,

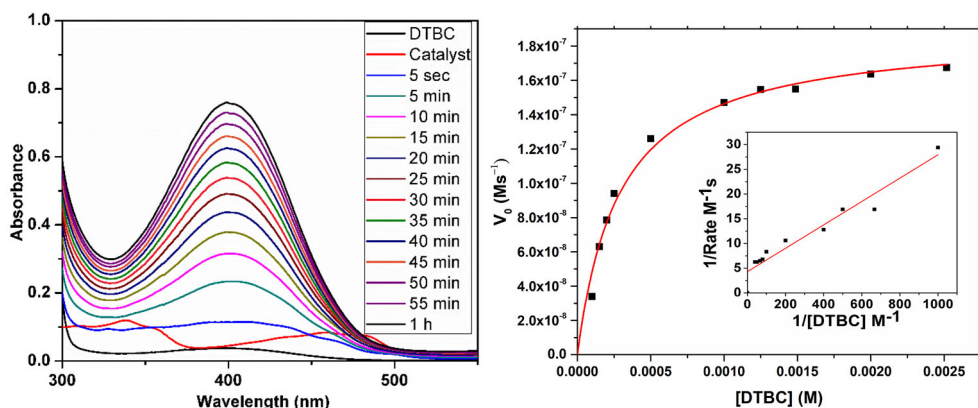


**Figure 6.** (a) Increase in absorption intensity with time after addition of 100 equivalent of 3,5-DTBCH<sub>2</sub> to a solution containing complex in **1** in DMF; (b) Initial rates vs [substrate] for the oxidation reaction by **1** as a catalyst in DMF. Lineweaver–Burk plot is given as inset.

corresponds to the metal centered Mn<sup>II</sup>-Mn<sup>II</sup>/Mn<sup>II</sup>-Mn<sup>III</sup> and Mn<sup>II</sup>-Mn<sup>III</sup>/Mn<sup>III</sup>/Mn<sup>III</sup> redox processes. In order to identify whether the catalytic oxidation is in fact catalyzed by **1**, a potential sweep of **1** (0.75 mM) was performed in the presence of catechol (15 equivalent) in the potential range  $-0.8$  V to  $+1.7$  V under nitrogen atmosphere. The voltammogram displayed an anodic peak at  $+0.93$  V corresponding to catechol oxidation, which is found to appear at the same potential in the absence of **1**. However, in the presence of oxygen a potential scan in the same potential window displayed an increase in catalytic current beyond  $+1.6$  V. This indicates that **1** catalyzes catechol oxidation in the presence of oxygen only (Figure S10, Supporting Information).

### 3.5. Catecholase activity of **1**

In most of the studies involving catechol oxidase activity, 3,5-di-tert-butylcatechol (3,5-DTBCH<sub>2</sub>) is used as a model substrate due to ease of oxidation of substrate to its corresponding quinone, 3,5-di-tert-butylquinone (3,5-DTBQ). No further oxidation is observed due to the bulkier groups present in the substrate [42]. The oxidized substrate 3,5-DTBQ also shows a characteristic strong absorption at *ca.* 400 nm which helps monitor the progress of the catalytic reaction. In order to study the catecholase activity of the manganese complex, a  $0.25 \times 10^{-4}$  M solution of complex in DMF was prepared and was treated with 100 fold of 3,5-DTBCH<sub>2</sub> in the same solvent (Figure 6a). The progress in the oxidation of the substrate under aerobic conditions was monitored by recording UV-visible spectra of the reaction mixture every 5 minutes up to a total time of 60 min after mixing. A gradual increase in the intensity of the spectra is an indication of the formation of more 3,5-DTBQ, which can be due to the catechol oxidase activity of the manganese complex. A control experiment performed in exactly the same conditions, without the manganese complex as the catalyst, show no change in the absorption intensity at 400 nm, indicating the absence of conversion of 3,5-DTBC into 3,5-DTBQ.

The kinetic study of the catalysis was monitored by performing a set of time-scans at the band maximum of the product (quinone) at a fixed temperature of 25 °C. The

**Table 3.** Comparison of catecholase activity by various compounds.

Catalyst	$V_{\max}$ ( $\text{Ms}^{-1}$ )	$K_M$ (M)	$k_{\text{cat}}$ ( $\text{h}^{-1}$ )	Ref.
Complex <b>1</b>	$(1.89 \pm 0.04) \times 10^{-7}$	$(2.89 \pm 0.26) \times 10^{-4}$	27.22	This work
$[\text{Mn}^{\text{II}}\text{L}(\text{OAc})(\text{H}_2\text{O})]\cdot\text{DMF}^{\text{a}}$	$(1.19 \pm 5.57) \times 10^{-7}$	$(7.73 \pm 1.5) \times 10^{-4}$	17.2	[23]
$[\text{Mn}^{\text{II}}\text{L}(\text{N}_3)(\text{H}_2\text{O})]^{\text{a}}$	$(1.76 \pm 0.6414) \times 10^{-7}$	$(10.2 \pm 1.4) \times 10^{-4}$	25.4	[23]
$[\text{Mn}^{\text{II}}\text{L}(\text{NCS})(\text{H}_2\text{O})]^{\text{a}}$	$(1.18 \pm 6.31) \times 10^{-7}$	$(6.22 \pm 1.5) \times 10^{-4}$	17.0	[23]
$[\text{Mn}_2(\text{O}_2\text{CCH}_3)(\text{N}-\text{C}_2\text{H}_5-\text{HPTB})](\text{ClO}_4)_2^{\text{b}}$	–	–	44	[45]
$[\text{Mn}_2(\text{O}_2\text{CC}_6\text{H}_5)(\text{N}-\text{C}_2\text{H}_5-\text{HPTB})](\text{ClO}_4)_2^{\text{b}}$	–	–	24	[45]
$[\text{Mn}_2(\text{O}_2\text{CCH}_3)(\text{H}-\text{HPTB})](\text{ClO}_4)_2^{\text{b}}$	–	–	8	[45]
$[\text{Mn}_2(\text{O}_2\text{CC}_6\text{H}_5)(\text{H}-\text{HPTB})](\text{ClO}_4)_2^{\text{b}}$	–	–	8	[45]
$[\text{Mn}(6 \text{ Me}_2\text{indH})(\text{H}_2\text{O})_2(\text{CH}_3\text{CN})](\text{ClO}_4)_2^{\text{c}}$	$23 \times 10^{-7}$	$12.7 \times 10^{-3}$	48.8	[44]
$[\text{Mn}^{\text{II}}(\text{bpy})_2(\text{H}_2\text{O})(\text{ClO}_4)](\text{ClO}_4)^{\text{d}}$	$(63.6 \pm 6.48) \times 10^{-4}$	$(36 \pm 1.04) \times 10^{-4}$	126.9	[46]
$[\text{Mn}^{\text{II}}_2\text{Mn}^{\text{III}}_4\text{O}_2(\text{pyz})_2(\text{C}_6\text{H}_5\text{CH}_2\text{COO})_{10}]_n^{\text{e}}$	$(7.076 \pm 16.2) \times 10^{-5}$	$(1.745 \pm 0.32) \times 10^{-4}$	2547	[43]

<sup>a</sup>L = N,N'-ethylenbis(3-ethoxysalicylaldimine), solvent DMF.

<sup>b</sup>HPTB = N,N,N',N'-tetrakis(2-benzimidazolylmethyl)-2-hydroxy-1,3-diaminopropane, solvent MeOH.

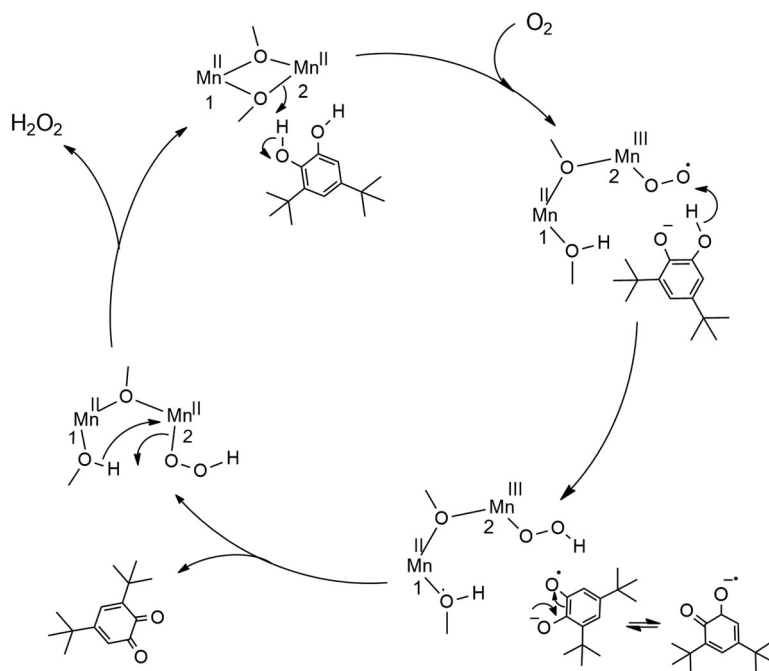
<sup>c</sup>6 Me<sub>2</sub>indH = 6'-methyl-2-pyridylimino)isoindoline, solvent DMF.

<sup>d</sup>bpy = bipyridine, solvent MeOH.

<sup>e</sup>pyz = pyrazine, solvent CH<sub>3</sub>CN.

concentration of the complex was kept constant at  $0.25 \times 10^{-4}$  M, and the concentration of the 3,5-DTBCH<sub>2</sub> varied from  $0.25 \times 10^{-3}$  M to  $0.25 \times 10^{-2}$  M. The initial rate method was used for determining the rate constant for the catalyst, complex **1**. At lower concentrations of the substrate, first-order kinetics were observed, indicating substrate-catalyst binding in the initial stage of the catalytic reaction [43]. The rate constant vs. substrate concentration was measured on the basis of the Michaelis–Menten equation to get the Lineweaver–Burk plot and the parameters  $V_{\max}$ ,  $K_M$  and  $K_{\text{cat}}$  (Figure 6b). A comparison of the catecholase activity of the manganese complex with other similar manganese-based catalysts reported in DMF is presented in Table 3. It can be observed that for a mononuclear manganese(II) complex, reported elsewhere, the  $K_{\text{cat}}$  value appears to be higher in DMF medium [23, 44]. For manganese(II) dinuclear complexes in methanol medium reported elsewhere [45], the turnover number is found to be lower than for **1** we have reported here. For a 1 D Mn(II) coordination polymer in methanolic medium the  $K_{\text{cat}}$  value is higher than those reported for mononuclear complexes [46], but is lower than the one observed in an Mn<sup>II</sup>/Mn<sup>III</sup> hexanuclear cluster [43]. It can be observed from the mass spectral data (Figure S11, Supporting Information) that the complex breaks down to a dinuclear species, which may be responsible for catecholase activity in solution. From the above observations, it can be concluded that the lower activity displayed by **1** may be due to the electron deficient nature of the ligand used.

The aerobic catechol oxidation reaction is generally assumed to involve the release of H<sub>2</sub>O<sub>2</sub> during the catalytic cycle. Therefore, to identify the presence of H<sub>2</sub>O<sub>2</sub> during catechol oxidation, the starch-iodide test was performed. For this test, a starch-potassium iodide mixture was added to the mixture of **1** and 3,5-DTBCH<sub>2</sub>. If H<sub>2</sub>O<sub>2</sub> is released during the catechol oxidation reaction, the hydrogen peroxide is expected to react with the potassium iodide releasing I<sub>2</sub>. The molecular iodine released forms an inclusion complex with starch, giving a blue color. In our experiment, the blue coloration was observed during the starch-iodide test, indicating the release of H<sub>2</sub>O<sub>2</sub>. Based on the above observation, a plausible mechanism of the catechol oxidation reaction by the manganese complex is suggested as given in Scheme 2. The catalytic cycle is initiated by the loss of the proton from the bridging methanol which then abstracts a



**Scheme 2.** A plausible mechanism for catechol oxidation under aerobic condition catalyzed by **1**.

proton from a hydroxyl group of the catechol, leading to the formation of methanol which remains coordinated to Mn<sub>1</sub>. The dioxygen then attacks the coordinatively unsaturated Mn<sub>2</sub>. The coordinated peroxide radical ion then abstracts the second phenolic hydrogen atom from the catecholate species. This leaves behind a phenolate radical ion which quickly rearranges to the DTBQ radical. The DTBQ radical is then quickly converted to free 3,5-DTBQ; the odd electron is likely to get transferred to the Mn(III) of the dinuclear Mn<sub>2</sub> core by tunnelling via the Mn(III)-peroxide bond. This is followed by the release of H<sub>2</sub>O<sub>2</sub> by the abstraction of a proton from coordinated methanol on Mn<sub>1</sub>, regenerating the catalytic Mn<sub>2</sub> core.

#### 4. Conclusion

A new manganese coordination polymer, [Mn<sup>II</sup><sub>2</sub>(L)<sub>2</sub>(MeOH)<sub>2</sub>]<sub>n</sub>, was synthesized from a tetradentate ligand H<sub>2</sub>L by a self-assembly process. The two manganese(II) metal ions are connected by two methanol molecules in a μ<sub>2</sub>-bridging mode. The dinuclear assembly is further linked via the pyridyl nitrogen atoms to form a three-dimensional coordination polymer. The network formed has 4-connected closed loops linked by 4-fold helical connectivity. The compound displays moderate catecholase like activity in aerobic condition with concomitant release of H<sub>2</sub>O<sub>2</sub>.

## Acknowledgements

The authors, PB and RJ, thank the Department of CSS, IACS Kolkata for facilitating X-ray single crystal data collection and PB thanks IIT(ISM) Dhanbad for financial support, National Taiwan University for XPS. The authors also acknowledge Dr. S.K. Padhi for cyclic voltammetry measurements and fruitful discussions.

## Disclosure statement

No potential conflict of interest was reported by the author(s).

## ORCID

Rohith P. John  <http://orcid.org/0000-0003-3175-027X>

## References

- [1] A. Sigel, H. Sigel. *Manganese and Its Role in Biological Processes. Metal Ions in Biological Systems*, Vol. 37, Marcel Dekker, New York (2000).
- [2] (a) K.D. Karlin, J. Tyeklár (Eds.), *Bioinorganic Chemistry of Copper*, Chapman & Hall, New York (1993);(b) G.C. Dismukes. *Chem. Rev.*, **96**, 2909 (1996);(c) M.M. Najafpour, S. Heidari, S.E. Balaghi, M. Hołyńska, M.H. Sadr, B. Soltani, M. Khatamian, A.W. Larkum, S.I. Allakhverdiev. *Biochim. Biophys. Acta*, **1858**, 156 (2017).
- [3] (a) T.N. Nguyen, M. Shiddiq, T. Ghosh, K.A. Abboud, S. Hill, G. Christou. *J. Am. Chem. Soc.*, **137**, 7160 (2015);(b) T.A. Jenkins, M. Garnero, S.A. Corrales, E.R. Williams, A.M. Mowson, A. Ozarowski, W. Wernsdorfer, G. Christou, C. Lampropoulos. *Inorg. Chem.*, **56**, 14755 (2017).
- [4] (a) W. Liu, K. Lee, M. Park, R.P. John, D. Moon, Y. Zou, X. Liu, H.-C. Ri, G.H. Kim, M.S. Lah. *Inorg. Chem.*, **47**, 8807 (2008);(b) R.P. John, M. Park, D. Moon, K. Lee, S. Hong, Y. Zou, C.S. Hong, M.S. Lah. *J. Am. Chem. Soc.*, **129**, 14142 (2007);(c) R.P. John, K. Lee, B.J. Kim, B.J. Suh, H. Rhee, M.S. Lah. *Inorg. Chem.*, **44**, 7109 (2005).
- [5] L. Radovanović, J. Rogan, D. Poleti, M.V. Rodić, N. Begović. *Inorg. Chim. Acta*, **445**, 46 (2016).
- [6] S.K. Dey, M. Hazra, L.K. Thompson, A. Patra. *Inorg. Chim. Acta*, **443**, 224 (2016).
- [7] L.E. Kreno, K. Leong, O.K. Farha, M. Allendorf, R.P. Van Duyne, J.T. Hupp. *Chem. Rev.*, **112**, 1105 (2012).
- [8] A.H. Chughtai, N. Ahmad, H.A. Younus, A. Laypkov, F. Verpoort. *Chem. Soc. Rev.*, **44**, 6804 (2015).
- [9] T.K. Maji, S. Sain, G. Mostafa, T.H. Lu, J. Ribas, M. Monfort, N.R. Chaudhuri. *Inorg. Chem.*, **42**, 709 (2003).
- [10] J.L. Manson, A.M. Arif, J.S. Miller. *Chem. Commun.*, 1479 (1999).
- [11] (a) H.J. Chen, Z.W. Mao, S. Gao, X.M. Chen. *Chem. Commun.*, 2320 (2001). (b) E.R.H. Wang, Q. Gao, M.C. Hong, S. Gao, J.H. Luo, Z.Z. Lin, L. Han, R. Cao. *Inorg. Chem.*, **42**, 5486 (2003).
- [12] H. Hosseini-Monfared, S. Alavi, P. Mayer. *Inorg. Chim. Acta*, **419**, 89 (2014).
- [13] P. Kar, A. Ghosh. *Inorg. Chim. Acta*, **395**, 67 (2013).
- [14] J.W. de Boer, W.R. Browne, J. Brinksma, P.L. Alsters, R. Hage, B.L. Feringa. *Inorg. Chem.*, **46**, 6353(2007).
- [15] H. Liang, Y.-X. Ji, R.-H. Wang, Z.-H. Zhang, B. Zhang. *Org. Lett.*, **21**, 2750 (2019).
- [16] (a) M.K. Singh, G. Rajaraman. *Inorg. Chem.*, **58**, 3175 (2019);(b) K.R. Vignesh, S.K. Langley, C.J. Gartshore, B. Mobaraki, K.S. Murray, G. Rajaraman. *Inorg. Chem.*, **56**, 1932 (2017).
- [17] C. Choe, Z. Lv, Y. Wu, Z. Chen, T. Sun, H. Wang, G. Li, G. Yin. *J. Mol. Catal.*, **438**, 230 (2017).

- [18] (a) J.-W. Wang, D.-C. Zhong, T.-B. Lu. *Coord. Chem. Rev.*, **377**, 225 (2018);(b) G. Maayan, N. Gluz, G. Christou. *Nat. Catal.*, **1**, 48 (2018).
- [19] G.N. Ledesma, H. Eury, E. Anxolabéhère-Mallart, C. Hureau, S.R. Signorella. *J. Inorg. Biochem.*, **146**, 69 (2015).
- [20] (a) D. Mondal, M.C. Majee. *Inorg. Chim. Acta*, **465**, 70 (2017);(b) A. Panja, N. Ch. Jana, S. Adak, K. Pramanik. *Inorg. Chim. Acta*, **459**, 113 (2017).
- [21] P. Halder, S. Paria, T.K. Paine. *Chem. Eur. J.*, **18**, 11778 (2012).
- [22] S. Paria, P. Halder, T.K. Paine. *Angew. Chem. Int. Ed.*, **51**, 6195 (2012).
- [23] P. Chakraborty, S. Majumder, A. Jana, S. Mohanta. *Inorg. Chim. Acta*, **410**, 65 (2014).
- [24] T.P. Camargo, F.F. Maia, C. Chaves, B. de Souza, A.J. Bortoluzzi, N. Castilho, T. Bortolotto, H. Terenzi, E.E. Castellano, W. Haase, Z. Tomkowicz, R.A. Peralta, A. Neves. *J. Inorg. Biochem.*, **146**, 77 (2015).
- [25] S. Majumder, S. Mondal, P. Lemoine, S. Mohanta. *Dalton Trans.*, **42**, 4561 (2013).
- [26] (a) C.-I. Yang, Z.-Z. Zhang, S.-B. Lin. *Coord. Chem. Rev.*, **289**, 289 (2015);(b) M. Mitra, A.K. Maji, B.K. Ghosh, G. Kaur, A.R. Choudhury, C.-H. Lin, J. Ribas, R. Ghosh. *Polyhedron*, **61**, 15 (2013);(c) Y. Gultneh, T.B. Yisgedu, Y.T. Tesema, R.J. Butcher. *Inorg. Chem.*, **42**, 1857 (2003);(d) X. Tang, J. Hua, H. Li, K. Jiang, L. Sun, Y. Ma, R. Yuan. *Inorg. Chim. Acta*, **441**, 126 (2016);(e) D.J. Fanna, Y. Zhang, L. Li, I. Karatchevtseva, N.D. Shepherd, A. Azim, J.R. Price, J. Aldrich-Wright, J.K. Reynolds, F. Li. *Inorg. Chem. Front.*, **3**, 286 (2016);(f) C.-G. Yan, M.-J. Zhu, J. Sun, W.-L. Liu, Y.-C. Shi. *J. Coord. Chem.*, **60**, 1083 (2007);(g) Y. Yang, L. Zhang, L. Liu, G. Liu, J. Guo, D. Jia. *Struct. Chem.*, **18**, 909 (2007).
- [27] S. Stoll, A. Schweiger. *J. Magn. Reson.*, **178**, 42 (2006).
- [28] D.R. Richardson, P.V. Bernhardt. *J. Biol. Inorg. Chem.*, **4**, 266 (1999).
- [29] N.S. Biradar, R.H. Raythatha, V.B. Mahale. *Curr. Sci.*, **45**, 124 (1976).
- [30] A. Ahmed, M. Dalia, H. Fatmaa. *Aust. J. Basic Appl. Sci.*, **9**, 42 (2015).
- [31] (a) G.M. Sheldrick, *SHELXT-2014/7, Program of Crystal Structure Solution*, University of Göttingen, Göttingen, Germany (2014);(b) G.M. Sheldrick. *Acta Crystallogr., Sect. A*, **71**, 3 (2015).
- [32] (a) G.M. Sheldrick, *SHELXL-2014/7, Program for the Solution of Crystal Structures*, University of Göttingen, Göttingen, Germany (2014);(b) G.M. Sheldrick. *Acta Crystallogr., Sect. C*, **71**, 3 (2015).
- [33] A.L. Spek. *Acta Crystallogr. C Struct. Chem.*, **71**, 9 (2015).
- [34] A.A. Gahr. *Spectrochim. Acta Part A*, **46**, 1751 (1990).
- [35] S.P. Sovilj, V.M. Vasić, D.L. Stojić, B. Stojčeva-Radovanović, L.T. Petkovska. *Spectrosc. Lett.*, **31**, 1107 (1998).
- [36] C. Zhan, J. Lu, A.J. Kropf, T. Wu, A.N. Jansen, Y.-K. Sun, X. Qiu, K. Amine. *Nat. Commun.*, **4**, 2437 (2013).
- [37] D. Asakura, Y. Nanba, M. Okubo, Y. Mizuno, H. Niwa, M. Oshima, H. Zhou, K. Okada, Y. Harada. *J. Phys. Chem. Lett.*, **5**, 4008 (2014).
- [38] (a) A. Saha, P. Majumdar, S. Goswami. *J. Chem. Soc., Dalton Trans.*, 1703 (2000);(b) P. Basu, A. Chakravorty. *Inorg. Chem.*, **31**, 4980 (1992);(c) S. Ganguly, S. Karmakar, C.K. Pal, A. Chakravorty. *Inorg. Chem.*, **38**, 5984 (1999).
- [39] A. Ray, C. Rizzoli, G. Pilet, C. Desplanches, E. Garribba, E. Rentschler, S. Mitra. *Eur. J. Inorg. Chem.*, **2009**, 2915 (2009).
- [40] P. Sarkar, A. Tiwari, A. Sarmah, S. Bhandary, R.K. Roy, C. Mukherjee. *Chem. Commun.*, **52**, 10613 (2016).
- [41] T.H. Bennur, D. Srinivas, P. Ratnasamy. *Microporous Mesoporous Mater.*, **48**, 111 (2001).
- [42] J. Mukherjee, R. Mukherjee. *Inorg. Chim. Acta*, **337**, 429 (2002).
- [43] P. Kar, R. Haldar, C.J. Gómez-García, A. Ghosh. *Inorg. Chem.*, **51**, 4265 (2012).
- [44] J. Kaizer, G. Baráth, R. Csonka, G. Speier, L. Korecz, A. Rockenbauer, L. Párkányi. *J. Inorg. Biochem.*, **102**, 773 (2008).
- [45] A.M. Magherusan, D.N. Nelis, B. Twamley, A.R. McDonald. *Dalton Trans.*, **47**, 15555 (2018).
- [46] S. Ganguly, P. Kar, M. Chakraborty, A. Ghosh. *New J. Chem.*, **42**, 9517(2018).